**2**

Paper 2

# Numerical study of an SOFC with direct internal reforming using charge diffusion-based model

Ho TX, Kosinski P, Hoffmann AC, Vik A

# Numerical Study of an SOFC with Direct Internal Reforming Using Charge Diffusion-Based Model

## Thinh X. Ho[1], Pawel Kosinski[1], Alex C. Hoffmann[1], Arild Vik[2]

[1]University of Bergen,  Department of Physics and Technology
Allegaten 55, NO-5007 Bergen, Norway
Tel.: +(47) 55574128
Email: thinh.ho@ift.uib.no
[2]Prototech AS, Fantoftvegen 38, NO-5892 Bergen, Norway

## Abstract

A unit planar, anode-supported solid oxide fuel cell (SOFC) with mixed-conducting electrodes is modeled and simulated. Direct internal reforming of methane is included in the model. In order to capture all macro and micro processes occurring in the cell, a single computational domain with fine mesh in the porous electrodes and the electrolyte membrane is created. On this domain the conservation of mass, momentum and species and energy coupled chemical and electrochemical processes are solved simultaneously. The computational package Star-CD is used together with subroutines developed in-house. The transport of oxygen ions within the ionically conducting phases of the electrodes and through the electrolyte is modeled by a Fickian diffusion processes.

Both co- and counter-flow configurations are investigated. The reforming and shift reactions are assumed to take place everywhere on the anode side, including the fuel channel, due to the high operating temperature (700-1000$^o$C). Note that the methane reforming reaction is endothermic and catalyzed by nickel particles. For the co-flow configuration, simulations with anodes of varying nickel loads are performed. It is found that an anode with low nickel load makes the temperature drop near the entrance of the cell less severe and thus mitigates thermal stresses in the cell. For the counter-flow case, results of chemical species, temperature and current density distribution are presented and discussed. For the same conditions as for the co-flow case, a very high peak appears on temperature profiles near the fuel entrance. The effects of varying inlet temperatures and flow rates are discussed.

# Introduction

A number of papers have addressed the problem of simulating the working of planar solid oxide fuel cells. In most of these papers (e.g. [1, 2, 3, 4, 5]) a current density is assumed and the losses in the cell are then worked out from empirical relations. Also thin electrodes and electrolytes are assumed in most of the literature. In this paper, we assume a voltage and work out the current density, using a diffusion process to mimic the effect of the electrical potential through electrodes and electrolyte of finite thicknesses.

The objective of this paper is to evaluate the performance of a planar solid oxide fuel cell with direct internal reforming at different flow configurations and fuel/air inlet conditions, using the above approach. The charge-diffusion model mimicking the effect of the potential in the cell has been presented elsewhere by the authors [6, 7], but will briefly be reviewed here. The commercial CFD package Star-CD is used. However, in order to make the simulations economical in terms of demands on time and computational power resources, only a part of a unit cell is considered. This part consists of a double gas channel sandwiching a positive electrode-electrolyte-negative electrode (PEN) structure. A schematic diagram of the model is shown in Figure 1.
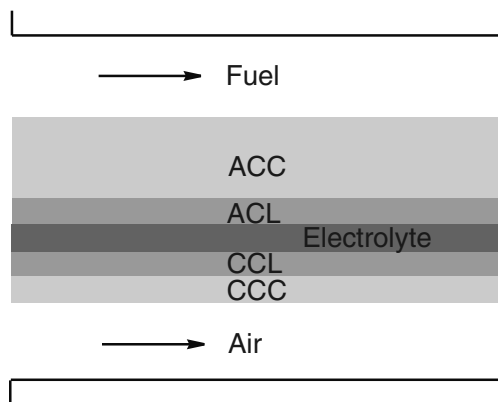


Figure 1: Schematic diagram of a unit anode-supported SOFC. ACC and CCC: anode and cathode current collectors, respectively; ACL and CCL: anode and cathode catalyst layers, respectively

The anode-supported design with co- and counter-flow configurations is investigated. Composites electrodes are used to increase the area of the electrochemically active sites. This is supposed to give a better performance of SOFCs. The electrolyte is made of the conventional material (YSZ) conducting oxygen ions. The electrodes consist of two layers, which are the current collector and the catalyst (active) layer where electrochemical processes occur. A single computational domain is created covering the two gas channels and the PEN structure. A finite volume-based mesh is generated over the domain.

# Mathematical model

Ideal gas mixtures and incompressible and laminar channel flows are assumed. Following is the system of governing equations [8]. Einstein summation convention is used. Subscripts $i$ and $j$ denote Cartesian coordinates and take on the values 1, 2 and 3.

Mass conservation:

$$\frac{\partial \epsilon \rho}{\partial t} + \frac{\partial \rho u_j}{\partial x_j} = 0 \tag{1}$$

Momentum equation for the channel flow:

$$\frac{\partial \rho u_i}{\partial t} + \frac{\partial}{\partial x_j} \left( \rho u_j u_i - \tau_{ij} \right) = -\frac{\partial p}{\partial x_i} + s_i \tag{2}$$

where $\epsilon$ is the porosity, $\rho$ is the gas mixture density, $u_j$ is the velocity component in direction $x_j$, $p$ is the pressure, $s_i$ is the momentum source components representing the sum of the body and other external forces ($s_i = 0$) and $\tau_{ij}$ is the tress tensor.

In the porous electrodes, the momentum balance of the gas permeation obeying Darcy's law and hence replaces Eq. (2):

$$\frac{\partial p}{\partial x_i} = -K_i U_i, \tag{3}$$

where $U_i$ is the superficial velocity, $K_i = \alpha_i |U| + \beta_i$ is the resistance due to the porous media. The coefficients $\alpha_i$ and $\beta_i$ are assumed to have the same values in the three different orthogonal directions and are taken as [9]:

$$\alpha = \frac{1.75 \rho \left( 1 - \epsilon \right)}{\epsilon^3 d_p}; \; \beta = \frac{150 \mu \left( 1 - \epsilon \right)^2}{\epsilon^3 d_p^2}, \tag{4}$$

which is consistent with the Ergun equation.

The species conservation equation:

$$\frac{\partial \epsilon \rho Y_m}{\partial t} + \frac{\partial}{\partial x_j} \left( \rho u_j Y_m + F_{m,j} \right) = s_m, \tag{5}$$

where $Y_m$ is the mass fraction of species $m$, $s_m$ the rate of mass production/consumption of species $m$ per unit volume due to chemical and/or electrochemical reactions and $F_{m,j}$ the Fickian diffusive mass flux of species defined as:

$$F_{m,j} = -\rho D_{m,j} \frac{\partial Y_m}{\partial x_j} \tag{6}$$

In an isotropic material, the Fickian diffusion coefficient, $D_m$, has the same value in all directions and is determined as

$$\frac{1}{D_m} = \frac{1}{D_{ml}} + \frac{1}{D_{mK}}, \tag{7}$$

where $D_{ml}$ is the ordinary binary diffusion coefficient of species $m$ in $l$ and $D_{mK}$ the Knudsen diffusion coefficient of species $m$. These are calculated by:

$$D_{ml} = 1.858 \cdot 10^{-7} \sqrt{\frac{1}{M_m} + \frac{1}{M_l}} \frac{T^{3/2}}{p \sigma_{ml}^2 \omega_D} \tag{8}$$

$$D_{mK} = \frac{d_p}{3} \sqrt{\frac{8RT}{\pi M_m}}, \tag{9}$$

where $M_m$ and $M_l$ are the molecular weights (g mol$^{-1}$) of species $m$ and $l$ respectively, $p$ is the total pressure (atm), $\sigma_{ml}$ (Å) and $\omega_D$ are Lennard-Jones parameters which can be found in common textbooks [9].

In porous media, $D_m$ is modified to take into account the tortuosity, $\tau$ and the result is called the effective diffusion coefficient, $D_m^{\text{eff}} = (\epsilon/\tau)D_m$.

The enthalpy equation for a solid or fluid of constant density:

$$\frac{\partial}{\partial t}(\epsilon \rho e) + \frac{\partial}{\partial x_j}(\rho u_j e + F_{h,j}) = \tau_{ij}\frac{\partial u_i}{\partial x_j} + s_h - s_c, \tag{10}$$

where $e = \bar{c}T - c_0 T_0$ is the specific internal energy, $s_h$ is the energy source due to e.g. ohmic resistances and radiation, $s_c$ is the chemical energy source accounting for endo- or exo-thermic chemical and electrochemical processes.

The diffusive thermal flux, $F_{h,j}$, is the combination of Fourier's conduction and the heat brought by the diffusive mass fluxes, defined as:

$$F_{h,j} = -k\frac{\partial T}{\partial x_j} + \sum_m h_{t,m}F_{m,j}, \tag{11}$$

where $k$ is the thermal conductivity of species mixture/material and $h_{t,m}$ is the specific thermal enthalpy of species $m$.

# Modeling of chemistry and electrochemistry

## Modeling of chemistry

The methane reforming and the shift reactions taking place in a solid oxide fuel cell operating with direct internal reforming are, respectively:

$$CH_4 + H_2O = CO + 3H_2 \tag{12}$$

$$CO + H_2O = CO_2 + H_2 \tag{13}$$

The heterogeneous reforming reaction (Eq.( 12)) is supposed to occur on the Ni-surface in the porous anode support, as well as in the three-phase boundary layer where Ni-particles are also present. The chemical species adsorption to and desorption from the Ni-surface are crucial processes of the reaction mechanism. The free surface of Ni-particles, therefore, contributes to the reaction rate [10]. However, since the diameter and thus the specific surface area of Ni-particles is not available, the reforming reaction rate is given in terms of Ni load [11]:

$$R_{\text{re}} = 1.75 \left(\frac{p_{\text{CH}_4}}{101325}\right)^{1.2} W_{\text{Ni}} \exp\left(\frac{-57840}{RT}\right), \tag{14}$$

where $R_{\text{re}}$ is computed in mol m$^{-3}$ s$^{-1}$, $p_{\text{CH}_4}$ (Pa) is the partial pressure of methane and $W_{\text{Ni}}$ (g m$^{-3}$) is the Ni load.

The reforming rate in the active layer is assumed to be two orders lower compared to that in the anode support zone in this study. This is because the free surface of Ni-particles is reduced by the appearance of the reactants and products of the electrochemical processes. Moreover, since the operating temperature of the cell is high (700–1000°C), the homogeneous reforming reaction can probably take place in the gas phase, within the fuel channel. A rate with three orders lower is thus assumed in the fuel channel.

Both products $H_2$ and CO of the reforming reaction are electrochemically active, however, the oxidation of the former is dominant over that of the later. Therefore, in this study CO is supposed to only take part in the shift reaction, which is kinetically strong and hence assumed to always be in equilibrium. The shift reaction will run forward in case $K > (p_{CO_2}p_{H_2})/(p_{CO}p_{H_2O})$, where $K$ is the equilibrium constant, producing $CO_2$ and $H_2$ while consuming CO and $H_2O$. The reaction runs backward in the opposite case.

## Modeling of electrochemistry

The reduction of $O_2$ (Eq. (15)) and the oxidation $H_2$ (Eq. (16)) taking place at the cathode and anode active layers, respectively, are presented as follows:

$$O_2 + 4e^- \rightleftharpoons 2O^{2-} \tag{15}$$

$$2H_2 + 2O^{2-} \rightleftharpoons 2H_2O + 4e^- \tag{16}$$

The overall cell reaction is:

$$H_2 + \frac{1}{2}O_2 = H_2O \tag{17}$$

The two half reactions (Eqs. (15) and (16)) can more generally be written:

$$Red \rightleftharpoons Ox + ne^- \tag{18}$$

The transfer current is calculated as the difference between the currents due to the forward and the backward reactions. This can be described by Butler-Volmer equation ([12, 13]):

$$j = A_{ac}i_0 \left\{ \exp\left( \beta\frac{nF\eta}{RT} \right) - \exp\left[ -(1-\beta)\frac{nF\eta}{RT} \right] \right\} \tag{19}$$

where $j$ is the transfer current per unit volume of active layer, $A_{ac}$ is the electrochemically active area per unit volume, $i_0$ is the exchange current density, $\beta$ is the transfer coefficient ($\beta = 0.5$), $n$ is the number of electrons participating in the electrochemical reaction, which is 2 for the reaction of Eq. (17), $F$ is Faraday's constant and $\eta$ is the activation overpotential. Note that $j$ is positive for anode where $H_2$ oxidation is dominant and negative for cathode electrode where $O_2$ reduction is dominant.

The activation overpotential is defined as:

$$\eta = \Delta\Phi - E_{rev} \tag{20}$$

where $\Delta\Phi = \Phi_e - \Phi_i$ is the electric potential difference between electronic and ionic phases of composite electrode, and $E_{rev}$ is the reversible potential of electrode given by [14]:

$$E_{rev,c} = \frac{RT}{4F}\ln p_{O_2} \tag{21}$$

for the cathode with $O_2$ reduction reaction, and

$$E_{\text{rev},a} = \frac{RT}{2F} \ln \left( \frac{p_{\text{H}_2\text{O}}}{K p_{\text{H}_2}} \right) \tag{22}$$

for the anode with $H_2$ oxidation reaction, where $K$ is the equilibrium constant of the overall reaction (Eq. (17)). Subscripts a and c stand for anode and cathode active layers, respectively.

With low activation overpotentials, applying the truncated Taylor series $e^x \approx 1 + x$ to Eq. (19) results in the kinetics of the two half charge-transfer reactions:

$$r = k_0 |\eta| \tag{23}$$

where $r = |j|/F$ is the reaction rate, computed in mol m$^{-3}$ s$^{-1}$ and $k_0 = 2A_{\text{ac}}i_0/RT$ is the rate coefficient.

Incorporating Eqs. (20), (21) and (22) into Eq. (23), we have the reaction rates for $O_2$ reduction reaction at the cathode active layer:

$$r_{\text{c}} = - \left[ \Delta\Phi_{\text{c}} - \frac{RT}{4F} \ln p_{\text{O}_2} \right] k_0 \tag{24}$$

and $H_2$ oxidation reaction at the anode active layer:

$$r_{\text{a}} = \left[ \Delta\Phi_{\text{a}} + E_0 - \frac{RT}{2F} \ln \left( \frac{p_{\text{H}_2\text{O}}}{p_{\text{H}_2}} \right) \right] k_0 \tag{25}$$

where $E_0 = (RT/2F)\ln K = -\Delta G/2F$ with $\Delta G$ is the Gibbs free energy of reaction given by Eq. (17).

The transfer of oxygen ions across the electrolyte membrane obeys the Nernst-Planck equation:

$$i = -D_{ch} z_i F \left( \frac{\partial C_{ox}}{\partial x} + z_i C_{ox} \frac{F}{RT} \frac{\partial \Phi}{\partial x} \right) \tag{26}$$

where $i$ (C m$^{-2}$ s$^{-1}$) is the current density due to the flow of oxygen ions, $C_{ox}$ (mol m$^{-3}$) is the oxygen ion concentration, $z_i = 2$ is the oxygen ion valence, $F$ and $R$ are Faradays and the ideal gas constant, $T$ is the temperature and $\Phi$ (V) is the electric potential. The first term represents Fickian diffusion in the presence of a concentration gradient, and the second ohmic transport in the presence of an electric potential gradient.

If one assumes that the charge transport is largely ohmic, and $C_{ox}$ is constant, the first term becomes negligible, and the current density, in terms of $C_{ch} = -z_i F C_{ox}$ becomes:

$$i = D_{ch} z_i C_{ch} \frac{F}{RT} \frac{\partial \Phi}{\partial x} = D_{ch} \frac{\partial z_i C_{ch} \frac{F}{RT} \Phi}{\partial x} \tag{27}$$

where we have made use of the fact that $C_{ch}$ is constant in the last equation.

Comparing this expression with the Fickian term in Equation (26), which is the first term on the right-hand-side, we see that if we define an "effective concentration", $C_{ch}^{eq}$:

$$C_{ch}^{eq} \equiv z_i C_{ch} \frac{F}{RT} \Phi \tag{28}$$

and then use Fickian diffusion to model a field-driven charge transport in the electrolyte.

6

We thus see that both for purely diffusional and purely field-driven charge transport in a membrane, a Fickian functional form can be used to model the transport, and this is the way we model the charge transport through the electrolyte in this work.

In fact, in this paper we do not yet attempt to use the physical diffusion coefficient, rather we fit $D_{ch}$ to obtain physically realistic results. This makes us free to convert potential over the electrolyte to an equivalent charge concentration by just using a unit conversion coefficient, $f$, while incorporating the other constants in the fitted value of $D_{ch}$. We then obtain:

$$dC_{ch}^{eq} = d\Phi \left( \frac{dC_{ch}^{eq}}{d\Phi} \right) = d\Phi f \tag{29}$$

where $f$ takes on the value -1 if $C_{ch}$ is in Fmol m$^{-3}$, and -96487 if $C_{ch}$ is in C m$^{-3}$.

Using Eq. (29), Ohm's law can be rewritten to:

$$i = -\lambda \frac{\partial \Phi}{\partial x} = -\frac{\lambda}{f} \frac{\partial C_{ch}^{eq}}{\partial x} = D_{ch} \frac{\partial C_{ch}^{eq}}{\partial x} \tag{30}$$

which has the form of Fick's first law with $i$ the flux of charge in C m$^{-2}$ s$^{-1}$ and $D_{ch} = -\lambda/f$, where $\lambda$ is the electrical conductivity of the electrolyte material, a "diffusion coefficient" for charges.

The generation of oxygen ions at the cathode, their transfer through the electrolyte and their removal due to the electrochemical reaction at the anode are processes in series. A decrease e.g. in the rate of the electrode reactions will cause a reduction of the transfer rate through the electrolyte, which means that there will be a decrease in the field there. Our diffusion process correctly reflects this, at least qualitatively.

Knowing

- the potential drop over the electrolyte (converting $C_{ch}^{eq}$ back to potential)

- the potential difference between the electrodes (which we fix, see below), and

- that the rates of production and consumption of oxygen ions at the cathode and anode, respectively, must be equal

-makes it possible to calculate the electrode potentials for cathode and anode, $\Delta\Phi_c$ and $\Delta\Phi_a$, for use in Eqs. (24) and (25) to find the electrochemical reaction rates.

To do this we repeat the the following iterative procedure until the profiles for $C_{ch}^{eq}$ have converged:

- Assume initial profiles for $C_{ch}^{eq}$, giving $\Delta\Phi_c$ and $\Delta\Phi_a$,

- compute the rates of electrochemical reactions from Eqs. (24) and (25),

- obtain new profiles for $C_{ch}^{eq}$.

The cell voltage is defined by the electric potential difference between cathode and anode current collectors [10, 15, 16, 17], which we assume to be constants due to large electrical conductivity of the materials. Additionally, and for simplicity, we fix the concentration of electrons as constant in the active layers. The electric potentials of the electronic phase

therefore become uniform throughout the electrodes. As a consequence, the cell voltage can be calculated by:

$$E_{\text{cell}} = \Phi_{e,c} - \Phi_{e,a} \tag{31}$$

where $\Phi_{e,c}$ and $\Phi_{e,a}$ are the potentials in the anode and cathode active layers, respectively, which are prescribed the values of $\Phi_{e,c} = 1.7$ V and $\Phi_{e,a} = 1.0$ V, for instance, for an operating cell voltage of 0.7 V.

# Results and discussion

The computational mesh is presented in Figure 2. Along the $x$-direction, the mesh consists of 200 even elements. Along the $y$-direction, it consists of 26 elements (8 in the channels, 4 in the electrolyte, 4 in the cathode and 10 in the anode). Note that they are evenly divided in each sub-domain. Along the $z$-direction, the mesh consists of only one element. Therefore the simulations can be considered two-dimensional in this study. The mesh of 5200 elements is supposed to be fine enough to capture all the transport, chemical and electrochemical processes occurring in the cell. The cell component dimensions can be found in Table 1.
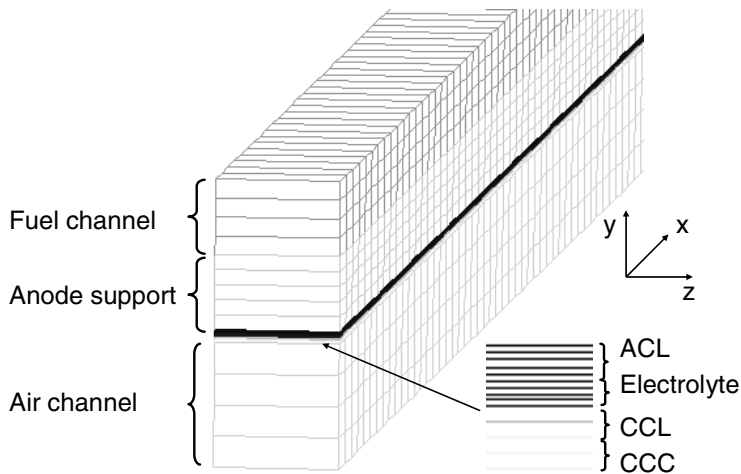


Figure 2: Computational mesh

Table 1: Dimensions of cell components

| Parameters | Value | Units |
|---|---|---|
| Cell width/length | 1/100 | mm |
| Air/Fuel channel height | 1/0.6 | mm |
| Anode active layer/current collector thickness | 30/0.6 | $\mu$m/mm |
| Cathode active layer/current collector thickness | 25/25 | $\mu$m |
| Electrolyte thickness | 20 | $\mu$m |

Table 2: Physical properties of cell components

| Parameters | Value | Units |
|---|---|---|
| Thermal conductivity, $k$ | | |
|    Anode/Cathode/Electrolyte | 4/4/10 | W m$^{-1}$ K$^{-1}$ |
| Electron diffusion coefficient, $D_{ch}$ | | |
|    Anode/Cathode | 0.311/0.133 | m$^2$ s$^{-1}$ |
| Oxygen charge diffusion coefficient, $D_{ch}$ | | |
|    Electrolyte | $0.881$exp$(-11000/T)$ | m$^2$ s$^{-1}$ |
|    Anode/Cathode active layer | $0.308$exp$(-11000/T)$ | m$^2$ s$^{-1}$ |
| Anode/Cathode porosity, $\epsilon$ | 0.4/0.3 | |
| Anode/Cathode tortuosity, $\tau$ | 1.6/1.6 | |
| Anode/Cathode pore diameter, $d_p$ | 2/1 | $\mu$m |
| Anode active layer density (Ni 50%wt.) | 4300 | kg m$^{-3}$ |

## Co-flow configuration

Results for chemical species and temperature distribution are presented in Figure 3. Model parameters and boundary and operating conditions can be found in Tables 2 and 3, respectively. As can be seen from Figure 3a which represented the chemical species in the fuel channel, in coming $CH_4$ is quickly reacted away, giving rise the content of $H_2$, which is then consumed by the electrochemistry. In this case the fuel utilization is 66.7%. However, the strongly endothermic reforming of methane consumes heat and hence reduces the temperature especially near the inlets (Figure 3b), causing high thermal stress in the cell. This effect can be mitigated by using extra air flow rate. However, the kinetics of the reforming reaction may probably have a contribution to this effect. This is discussed in the next section.
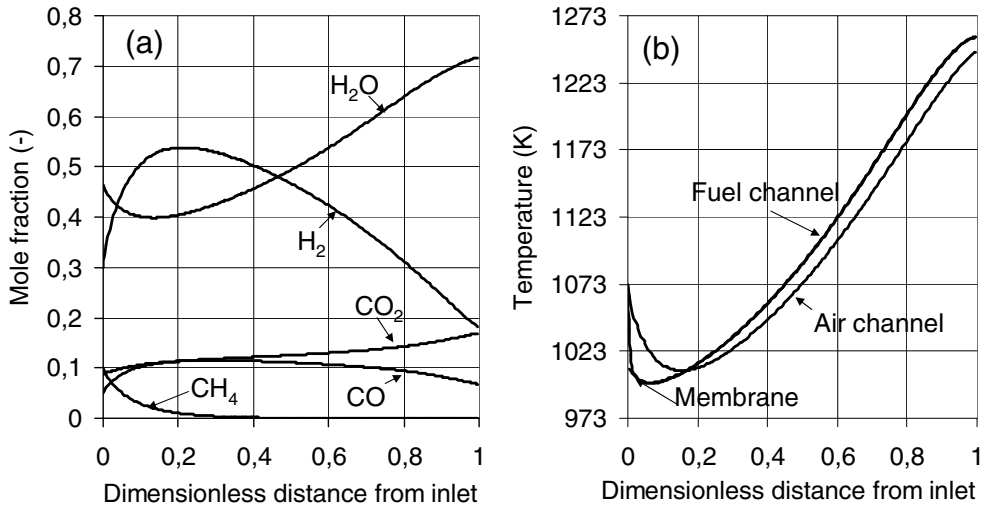


Figure 3: Evolution of chemical species (a) and temperature (b) along the cell length - the co-flow case [7]

## Effect of Ni load

Simulations with anode of different contents of nickel are performed. All parameters are kept the same as for the case above except the Ni-load. Results of methane conversion are presented and compared in Figure 4. The higher the nickel content is, the faster the methane is consumed. This effect can also be seen via the temperature and current density distribution demonstrated in Figure 5. With lower content of Ni (40% wt.) in the anode, the effect of sub-cooling is mitigated, and hence reducing the thermal stress. Additionally, in terms of cell performance, the average current density slightly increases with decreasing nickel load. It is 0.502, 0.505 and 0.509 A cm$^{-2}$ corresponding to the anode of 60, 50 and 40% Ni.
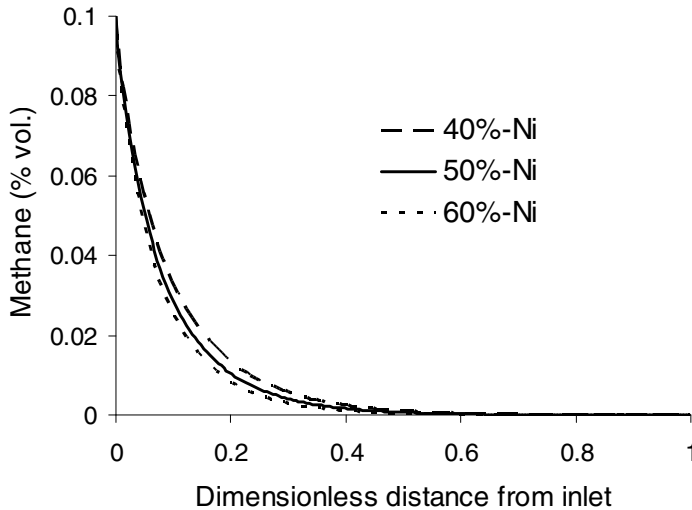
Figure 4: The conversion of methane at different Ni-loads along the fuel channel
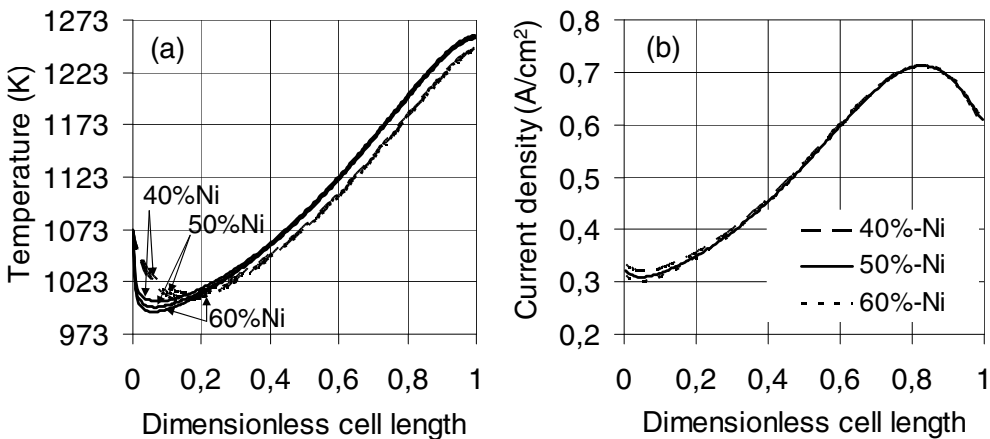
Figure 5: Distribution of temperature (a) and current density (b) at different Ni-loads along the cell length

Table 3: Boundary and operating conditions

| Parameters | Value and units |
|---|---|
| Fuel inlet velocity/Temperature | 0.3 m s$^{-1}$/1073 K |
| Fuel compositions | $H_2O$ 46.3%, $H_2$ 30%, |
| | $CH_4$ 10%, CO 5%, $CO_2$ 8.7% |
| Air inlet velocity/Temperature | 2.93 m s$^{-1}$/1073 K |
| Air compositions | $O_2$ 21%, $N_2$ 79% |
| Walls | no-slip, adiabatic |
| Cell voltage | 0.7 V |
| Rate coefficient, $k_0$ | $1.995 \cdot 10^6 \exp\left(-50000/RT\right)$ |

## Counter-flow configuration

The direction of air flow is now turned to the opposite direction. All parameters used for the counter-flow configuration are kept the same as for the co-flow case. These can be found in Tables 1, 2 and 3. Results for chemical species distribution in the fuel channel are presented in Figure 6. Compared to the co-flow case with the same working conditions, methane in the counter-flow case is reacted away faster, within 10% instead of around 20% of the channel length. The fuel utilization for this is as high as 86%. Results for temperature and current density distribution are demonstrated in Figure 7.
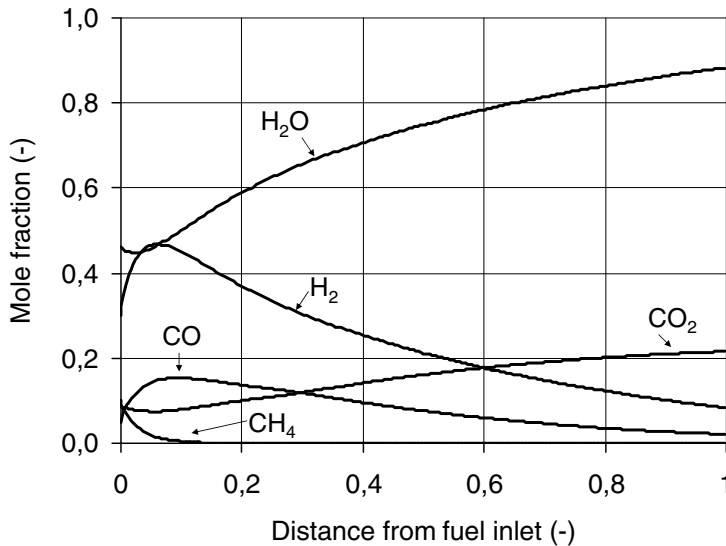


Figure 6: Evolution of chemical species in the fuel channel - the counter-flow case

As can be seen from Figure 7a, a very high peak of temperature appears near the entrance of the fuel channel, causing a high thermal stress in the cell. This is probably because the temperature at the two ends of the cell is fixed. The heat generated by the electrochemical processes is carried by the air flow with high velocity (convection), creating a high temperature zone downstream of the air flow. The current density curve along the cell length
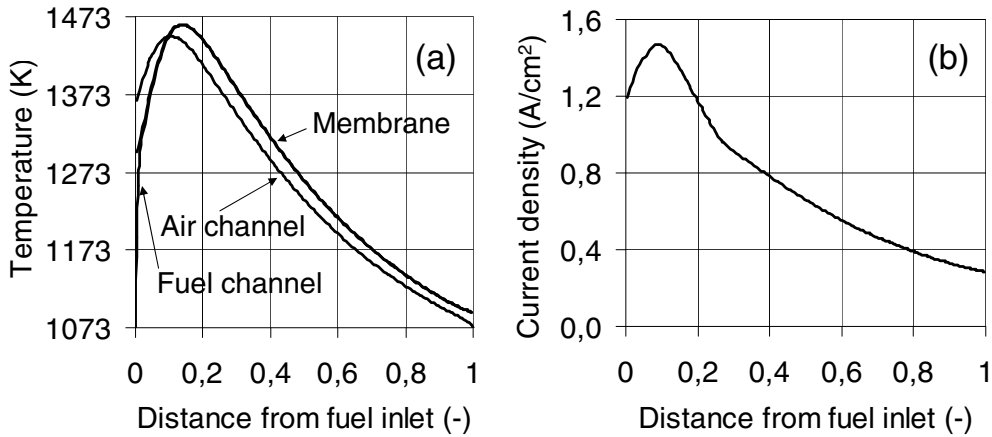
Figure 7: Distribution of temperature (a) and current density (b) along the cell length - the counter-flow case

(Figure 7b) has a similar trend with the temperature, with a high peak near the fuel entrance. However, it rapidly decreases along the fuel channel as long as $H_2$ is consumed.
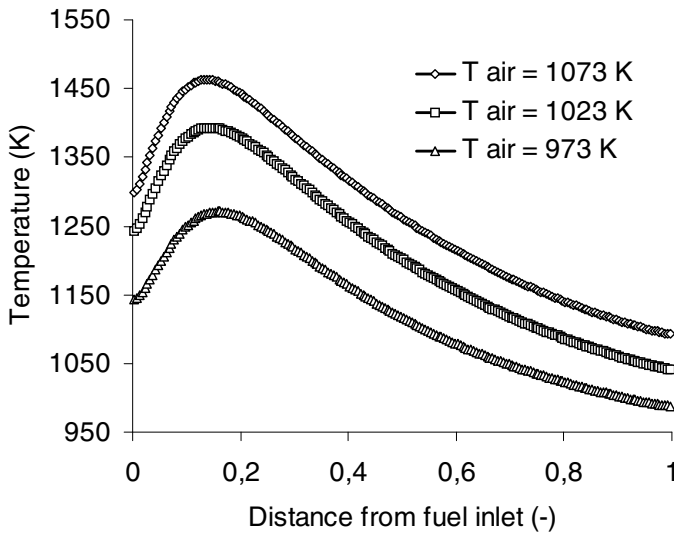


Figure 8: Membrane temperature along the cell length at different air inlet temperatures

Figure 8 shows the temperature of the electrolyte membrane with different inlet temperatures of the air flow. It is seen that a lower inlet temperature of the air flow can reduce the extremely rise of temperature and hence lessen the overall thermal stress in the cell. Moreover, the use of extra air flow rate may probably be a choice to mitigate the thermal stress and give a more uniformly distributed current density in the cell. This is true for SOFCs with co-flow configuration. Results for temperature and current density distribution along the cell length at different air inlet velocities are presented in Figure 9.
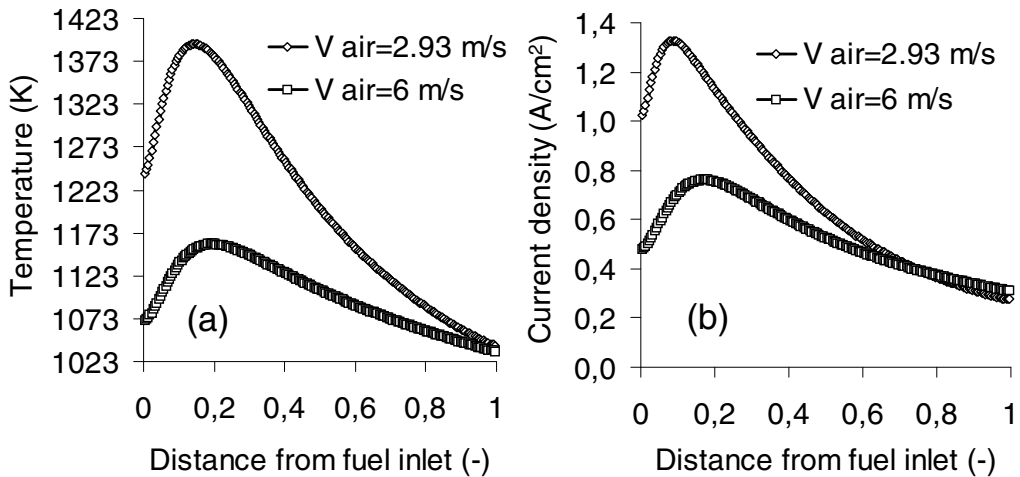
Figure 9: Distribution of the membrane temperature (a) and current density (b) along the cell length at different air inlet velocities - Air inlet at 1023 K

# Conclusions

A planar anode-supported solid oxide fuel cell with co- and counter-flow configurations has been investigated. Direct internal methane reforming was included. In the paper, the charge diffusion-based model was applied and implemented in the commercial CFD package Star-CD. It is found that with the co-flow configuration, nickel load on the composite anode can contribute to the sub-cooling effect near the fuel/air inlet. A low nickel load gives a less severe sub-cooling, and hence a better performance of the cell.

However, in the counter-flow case at otherwise the same working conditions as for co-flow, an extremely high temperature appears near the fuel entrance, resulting in severe thermal stresses both locally and overall. Nevertheless, lowering the inlet temperature of the air flow and/or using an extra air flow rate can reduce the thermal stresses. A current density which is more uniformly distributed along the cell length can therefore be obtained.

# Acknowledgments

# References

[1] J. R. Ferguson, J. M. Fiard, R. Herbin, Three-dimensional numerical simulation for various geometries of solid oxide fuel cells, Journal of Power Sources 58 (1996) 109–122.

[2] P. Aguiar, D. Chadwick, L. Kershenbaum, Modelling of an indirect internal reforming solid oxide fuel cell, Chemical Engineering Science 57 (2002) 1665–1677.

[3] M. Roos, E. Batawi, U. Harnisch, T. Hocker, Efficient simulation of fuel cell stacks with the volume averaging method, Journal of Power Sources 118 (2003) 86–95.

[4] K. P. Recknagle, R. E. Williford, L. A. Chick, D. R. Rector, M. A. Khaleel, Three-dimensional thermo-fluid electrochemical modeling of planar SOFC stacks, Journal of Power Sources 113 (2003) 109–114.

[5] W. G. Bessler, S. Gewies, M. Vogler, A new approach for elementary-kinetic modeling of internal-reforming SOFCs, in: Proceedings of the Tenth International Symposium on SOFCs (SOFC-X), Nara, Japan, 2007.

[6] T. X. Ho, P. Kosinski, A. C. Hoffmann, I. Wærnhus, A. Vik, Numerical simulation of electrochemical and transport processes in solid oxide fuel cells, in: ECS Transactions, Vol. 7(1), 2007, pp. 1901–1908.

[7] T. X. Ho, P. Kosinski, A. C. Hoffmann, A. Vik, Numerical modeling of solid oxide fuel cell, (Submitted).

[8] Star-CD, Version 3.24 Methodology, CD adapco Group, 2004.

[9] R. B. Bird, W. E. Stewart, E. N. Lightfoot, Transport phenomena, 2nd Edition, John Wiley and Sons, New York, 2002.

[10] H. Zhu, R. J. Kee, V. M. Janardhanan, O. Deutschmann, D. G. Goodwin, Modeling elementary heterogeneous chemistry and electrochemistry in solid oxide fuel cells, Journal of The Electrochemical Society 152 (2005) A2427–A2440.

[11] S. Nagata, A. Momma, T. Kato, Y. Kasuga, Numerical analysis of output characteristics of tubular SOFC with internal reformer, Journal of Power Sources 101 (2001) 60–71.

[12] V. S. Bagotsky (Ed.), Fundamentals of Electrochemistry, 2nd Edition, John Wiley & Sons, 2006, Ch. 6.

[13] E. Chan, Thermodynamics and electrochemical kinetics, in: G. Hoogers (Ed.), Fuel Cell Technology Handbook, CRC Press, 2003, Ch. 3.

[14] R. Suwanwarangkul, E. Croiset, M. D. Pritzker, M. W. Fowler, P. L. Douglas, E. Entchev, Mechanistic modelling of a cathode-supported tubular solid oxide fuel cell, Journal of Power Sources 154 (2006) 74–85.

[15] W. G. Bessler, S. Gewies, M. Vogler, A new framework for physically based modeling of solid oxide fuel cells, Electrochimica Acta 53 (2007) 1782–1800.

[16] C. Y. Wang, Fundamental models for fuel cell engineering, Chem. Rev. 104 (2004) 4727–4766.

[17] H. Zhu, R. J. Kee, Modeling distributed charge-transfer processes in membrane electrode assemblies with mixed-conducting composite electrodes, in: ECS Transactions, Vol. 7(1), 2007, pp. 1869–1878.